AMETHYST FROM NEWFOUNDLAND, CANADA: GEOLOGY, INTERNAL FEATURES, AND FLUID INCLUSION MICROTHERMOMETRY

Joshua William Lloyd Maloney, Philippe M. Belley, and James Conliffe

Gem-quality amethyst at the La Manche deposit in the Avalon Zone of Newfoundland, Canada, occurs in a calcite-galena-barite-quartz vein adjacent to a historical lead mine containing similar mineralization. The deposit has produced mineral specimens as well as medium to medium-dark purple (up to 11 ct) and light purple (<3 ct) faceted stones. Amethyst is interpreted to have formed as the final stage of hydrothermal mineral deposition in the veins. Variable color, zoning, and crystal size in different but contiguous crystal-lined pockets suggest relatively closed-system behavior within pockets where amethyst/quartz was deposited from trapped silica- and iron-bearing hydrothermal fluid. Microthermometry of primary fluid inclusions revealed an average homogenization temperature of 75.5 ± 6.9°C, cooler than in fluid inclusions within sulfide-bearing zones of similar veins in the region. Average fluid salinity estimated from primary inclusions in amethyst, recorded in weight % NaCl equivalent, was 10.7 ± 1.8 eq. wt.% NaCl. This was similar to the salinity of fluid in sulfide-bearing veins in the region and significantly higher than in quartz-chlorite veins in the region. Secondary fluid inclusions suggest a late influx of lower-salinity fluids (~7 eq. wt.% NaCl) associated with post-crystallization deformation that internally fractured amethyst crystals, reducing the volume suitable for faceting. Mineral inclusions are most abundant in the final purple and colorless growth stages in amethyst. They consist of black to red hematite spherulites, acicular "beetle-leg" inclusions (likely hematite), pyrite, chalcopyrite, and sprays of ochre goethite. Late iron-rich accessory mineral deposition may have depleted the hydrothermal fluid of iron, the chromophore in amethyst, during the final growth stage. La Manche amethyst's inclusion mineralogy is similar to that of amethyst from the deposits at Thunder Bay (Ontario, Canada), but the morphology of accessory sulfide minerals is different.

A new discovery of gem- and specimen-quality amethyst was made in Newfoundland, Canada, by Jason White in 2017 while conducting near-surface exploration in the proximity of a historical epigenetic vein-hosted lead deposit at La Manche, near Arnold's Cove. Amethyst, the purple variety of quartz colored by interstitial Fe^{3+} (Cohen, 1985), forms in a number of geological settings, but always at relatively low temperature (≤400°C) and shallow crustal depth (Cohen, 1985; McArthur et al., 1993; Yang et al., 2001; Kievlenko, 2003; Gilg et al., 2014). While gem-quality amethyst is known to occur in miarolitic granite pegmatites and skarns (Yang et al., 2001; Kievlenko, 2003; Ontiveros et al., 2004), commercially important deposits are hosted either in geodes within basalt or in epigenetic hydrothermal veins (Kievlenko, 2003). The purpose of this study is to (1) describe the amethyst gemstones and mineralization at La Manche, (2) identify amethyst's position in the paragenetic sequence of the veins, (3) characterize the mineral inclusions, (4) gain insights into formation temperature and hydrothermal fluid salinity by conducting fluid inclusion microthermometry on primary and secondary inclusions, and (5) use these data to develop an understanding of this new gem-quality amethyst occurrence and how it compares, geologically and gemologically, to others.

Regional Geology. La Manche is located in the Clarenville area of southeastern Newfoundland and situated in the Avalon Zone, a geological terrane that makes up the southeast part of Newfoundland (figure 1). Bedrock in this area is late Proterozoic in age, con-

See end of article for About the Authors and Acknowledgments.
GEMS & GEMOLOGY, Vol. 60, No. 3, pp. 348–367,
http://dx.doi.org/10.5741/GEMS.60.3.348

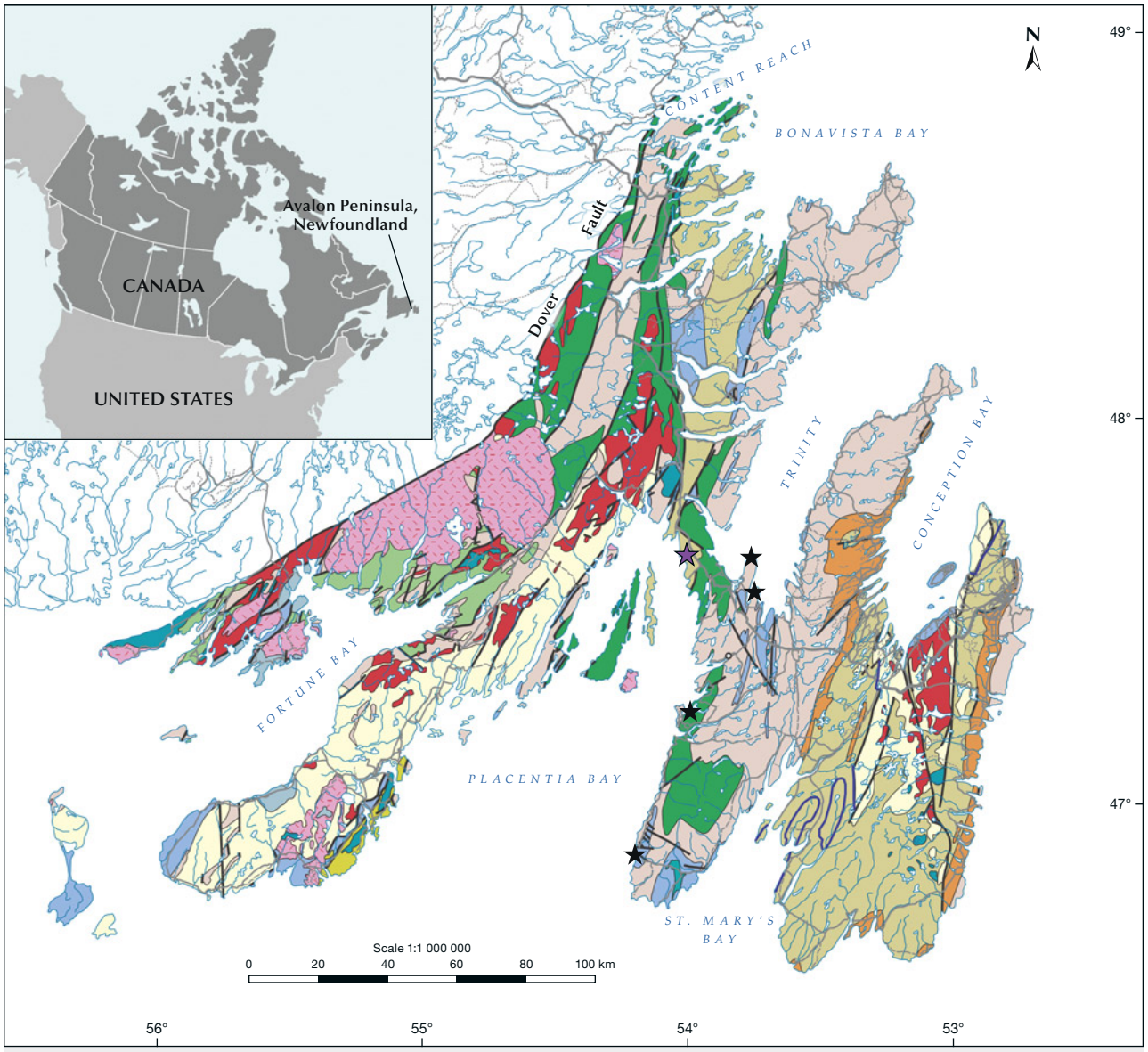

Figure 1. Geological map of the Avalon Zone showing the location of the La Manche vein system and other barite-bearing veins. Modified after Mills et al. (2021) and Colman-Sadd et al. (1990), with data from Maloney (1990).

sisting of clastic sedimentary rocks (turbidites formed in a marine basin; Mills et al., 2021) from the Connecting Point Group that are overlain by subaerial bimodal volcanic rocks of the Bull Arm Formation (Maloney, 1990). The Connecting Point Group consists of turbidites from a preserved marine sedimentary basin. Its oldest portion is constrained by the age of the underlying Love Cove Group, determined as 620 million years (Ma), and the 605 Ma age of a Bull Arm Formation rhyolite overlying the angular unconformity with the Connecting Point Group (O'Brien et al., 1989; Mills et al., 2016, 2021).

In Brief

- Gem-quality amethyst occurs as a late-stage mineral in an epigenetic hydrothermal calcite-galena-barite-quartz vein at La Manche on Placentia Bay in Newfoundland, Canada.
- Faceted stones from the occurrence range from light purple (<3 ct) to medium-dark purple (up to 11 ct). Color zoning is present but usually not very apparent in cut stones.
- Fluid inclusion microthermometry indicates that the amethyst formed at low temperature (<100°C) in NaCl-bearing fluids of moderate salinity (10.7 ± 1.8 eq. wt.% NaCl).
- Mineral inclusions in La Manche amethyst consist of spherulitic and acicular hematite, goethite sprays, pyrite, and chalcopyrite.

Within the Avalon Zone, a number of hydrothermal mineral veins occur (figure 1), consisting of barite, calcite, and sulfides—primarily galena with minor to trace sphalerite and chalcopyrite (Maloney, 1990). Maloney recognized two varieties of veins in the region: an early set of quartz ± chlorite veins (formed as a result of low-grade metamorphism) and a later set of barite ± calcite ± sulfide veins. Sulfide-bearing veins in La Manche and Silver Cliff (45 km south of La Manche, also in the Avalon Zone) are part of the subsequent set. Both deposits occur proximal to each other and are relatively rich in galena. Barite-bearing veins occur in other areas of the Avalon Peninsula such as Collier Point and Bellevue. Vein formation is interpreted to have taken place during or after the Acadian Orogeny (Devonian Period), when Avalon Zone rocks were weakly metamorphosed to sub-greenschist facies (prehnite-pumpellyite facies; Papezik, 1974), folded, faulted, and intruded by syntectonic to post-tectonic granites (Maloney, 1990).

La Manche Geology. The La Manche vein consists of an epigenetic vein-hosted lead deposit. Due to the abundance of galena, underground mining for lead was conducted by Ripley & Company, Placentia Bay Lead Company, and La Manche Mining Company from 1857 to 1873, followed by several unsuccessful attempts to resume mining operations between 1873 and 1948 (Tibbo, 1983). Large vugs described as containing "amethystine" quartz crystals along with transparent quartz were encountered during underground mining in the 1800s (Murray, 1869; Howley, 2009). The La Manche vein consists primarily of calcite and galena with subordinate barite, quartz, sphalerite, and chalcopyrite, and it is confined to the Connecting Point Group siltstone. The vein ranges from several centimeters to 3 m wide and occurs mostly within or at the contact of an amygdaloidal[1] basic dike (Maloney, 1990).

Maloney described various stages of white, gray, and purple calcite occurring in the vein. Previous research focused on the calcite along with barite and subordinate sulfides. He concluded, based on geological, geochemical, isotopic, and fluid inclusion evidence, that the sulfide-rich veins such as La Manche (and Silver Cliff) formed by a later and hotter hydrothermal fluid pulse closer to the source of fluids relative to the earlier quartz-chlorite veins in the Avalon Peninsula. Exsolved fluid from crystallizing magma belonging to nearby granitoids (Late Proterozoic; Colman-Sadd et al., 1990) is hypothesized to be the source of hydrothermal fluids forming barite- and sulfide-bearing veins in the region (Maloney, 1990).

In the early 1980s, exploration, trenching, and drilling identified a parallel vein 185 m north of the trace of the main La Manche vein. Amethyst was discovered in a drill core at approximately 18.5 m depth (Tibbo, 1983), in what has now been recognized as a significant amethyst occurrence described below.

Description of the Amethyst Occurrence. Jason White's 2017 discovery of amethyst occurred in a vein similar to the historically mined vein and is located near that deposit. The La Manche amethyst occurrence is currently in the exploration stage, with several test samples taken to evaluate mineral specimen and gem rough distribution and potential. A preliminary assessment of gemstone potential at La Manche was briefly described by Wilson (2020).

[1]An igneous dike containing amygdules, which are formed from the late filling of vesicles by minerals.

Figure 2. View of the amethyst-bearing trench looking west-southwest into Placentia Bay. The vein is exposed in the right side of the trench, and overburden is displaced to the left. Aerial drone photo by Philippe Belley.

Faceted amethyst from La Manche is occasionally found in the Canadian market as loose stones or set in silver jewelry. Future production potential is still under evaluation.

The strike and dip of the new amethyst-bearing vein is similar to that of the mined vein. No amygdaloidal dike was observed in outcrop at this location. The amethyst-producing vein is exposed by a 150 m long trench (figures 2 and 3). The vein dips steeply to the northwest and has a variable strike ranging from 203° to 264° based on measurements taken in four different segments of the trenched area. The average strike is similar to the orientation of the northern boundary of the trench (~244°), which appears to define the contact with the hanging wall. Amethyst was recovered mainly in the elongated flooded trench on the central-eastern part of the pit (figure 3), and small amounts were observed in the western part. Between these zones, the vein appears to pinch down to approximately 20 cm in width, but the poor exposure makes it difficult to follow the trace across the pit. The hanging wall consists of the host Connecting Point Group siltstone, which also occurs sparsely as fragments within the vein overgrown by layered calcite.

The vein exposed in the main area has a thickness of at least 2 m and consists of approximately 10–30 cm thick layers of columnar calcite (often highly weathered) containing localized galena masses, some up to ~1 m in diameter and 20 cm thick. The galena is extremely coarse-grained (5–15 cm) with a light greenish alteration coating likely composed of anglesite and subordinate pyromorphite. Galena masses, radiating white barite blades, and rare chalcopyrite occur in the calcite. Crystal-lined pockets are primarily hosted within the calcite—rarely do these pockets contain only euhedral calcite. More commonly, they are lined with a layer of barite followed by amethyst or colorless quartz (figure 4). Amethyst rarely forms directly over galena and uncommonly

Figure 3. Left: The trench face in the main zone (in 2021) showing amethyst-bearing black mud in front of the vein's hanging wall. Right: Freshly recovered amethyst cluster in black and tan mud. Many clusters are completely obscured by the thick black to brown clay. Photos by Philippe Belley.

does so on granular massive white quartz. Quartz crystals consist of short-prismatic points dominated by termination faces oriented growing inward in open cavities. Bright medium purple to dark intense purple (e.g., figure 3, right) amethyst crystals averaging 2–3 cm wide and up to 6 cm wide are the most common, and these colors are found in approximately equal proportions at the locality. Less common are smaller light purple (light purple core with thick colorless outer zone) and colorless quartz crystals, which may occur in pockets relatively close to those containing the more saturated colors of amethyst. An individual pocket tends to contain only one type of amethyst (i.e., colorless, light purple, medium purple, or dark purple) except for small (<1 cm) secondary colorless quartz crystals that are uncommonly found in small amounts over main generation quartz/amethyst of any color. These pockets are usually elongated roughly parallel to the vein and reach at least 1.5 m in length. Much of the calcite is intensely weathered into black clay with local, tan-colored zones and is mixed with masses of galena, barite, and quartz. There is considerable evidence of amethyst pocket collapse, movement, and resettling within the black clay. Post-formation collapse is suggested by a specimen of amethyst covered by cemented "crystal mush," which appears to precede calcite weathering and black clay formation. This deformation and the displacement of crystal clusters within the black clay resulted in damage to many amethyst crystals. Undamaged specimens are more common in less affected areas of the vein, especially near the hanging wall.

Figure 4. A portion of the vein showing thick calcite (Cal) and massive galena (Gn) surrounding a pocket of barite (Brt) and amethyst (Qtz). Photo by Joshua Maloney.

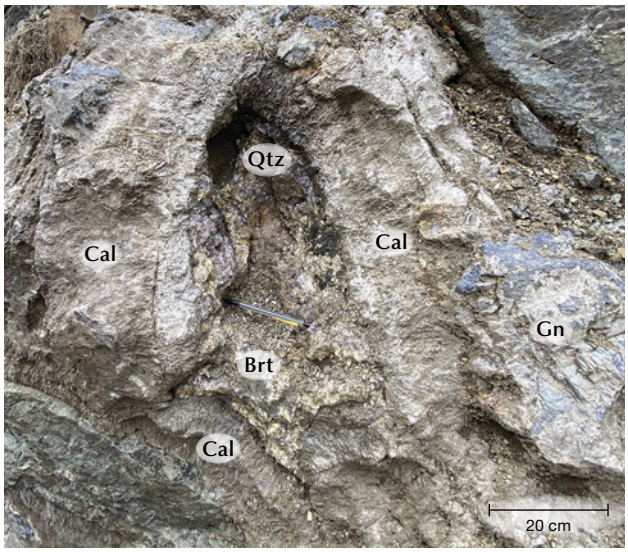

MATERIALS AND METHODS

Samples. More than 100 amethyst clusters were examined in addition to hundreds of faceted gemstones. These were collected by the claim owner and some of the authors (PB and JM) as part of a test sampling program, with rough being faceted in a commercial cutting factory. Approximately 2.4 kg out of a 7.0 kg sample of loose amethyst crystals recovered from the main zone consisted of facetable rough. The rough amethyst crystals were mostly medium-dark purple, with some medium purple varieties. These were faceted as calibrated round brilliant stones, each 5 mm in diameter or larger. Custom precision cutting was reserved for higher-quality rough. The 2.4 kg of amethyst loose crystals produced a total of 357 faceted stones: 164 stones weighing ≥1.0 ct (custom cuts and 7–10 mm round brilliants, maximum 6.42 ct, average 1.66 ct) and 193 stones weighing <1.0 ct (5–6 mm round brilliants, average 0.59 ct). Gemstones are described further in the Results section below. A subset of samples was selected for more detailed study: Seven crystals were prepared as polished sections for fluid inclusion analysis (samples LM-Ame-1 to LM-Ame-7, five of which contained fluid inclusions suitable for analysis), and 12 gemstones with characteristic inclusions were selected for photography and characterization.

Sample Examination and Preparation. Selected gemstones were observed under magnification with a binocular microscope. Three amethyst crystals and two barite-calcite contacts were polished into slide-mounted polished sections and studied using a petrographic microscope and a scanning electron microscope. These sections as well as included gemstones (broken and repolished to expose inclusions) were carbon coated (coating thickness 5–10 nm) and examined using Memorial University of Newfoundland's FEI Quanta 650 SEG scanning electron microscope (SEM). The SEM was equipped with two Bruker XFlash 5030 energy-dispersive X-ray spectrometers (EDS) for mineral identification using an operating voltage of 25 kV and an X-ray acquisition time of 30 s. Reference examples of hematite and goethite were mounted and polished together with included amethyst samples in a 25 mm epoxy puck so that the inclusions could be accurately identified. Refractive indices were measured using a Kruss professional refractometer with a monochromatic sodium light source (an RI liquid with a high value of 1.81, consisting of methylene iodide and tetraiodoethylene, was used at the contact face). Specific gravity was measured hydrostatically.

Fluid Inclusion Petrography and Microthermometry. Fluid inclusion assemblages (FIA) were identified and classified using criteria outlined by Goldstein (2003):

1. Primary inclusions are trapped during crystal growth and commonly found along growth layers and elongate in the direction of crystal growth.
2. Secondary inclusions form after crystal growth from fractures or deformation features that heal, thereby trapping the inclusions. These inclusions cut across growth zones.
3. Pseudosecondary inclusions are similar to secondary inclusions but form before crystal growth has finished. They form along deformation features that occur before the crystal has finished growing.

In addition, some clusters of inclusions have no clear relationship to growth zones but are not in fractures of clearly secondary or pseudosecondary origin. These inclusions are classified as having an indeterminate origin.

Seven saturated medium-dark purple amethyst crystals (LM-Ame-1 to LM-Ame-7) were fabricated into doubly polished wafers for fluid inclusion examination and analysis. Microthermometric data was collected using a Linkam THMSG600 heating/cooling stage attached to an Olympus BX51 microscope at Memorial University of Newfoundland. The heating/cooling stage was calibrated using synthetic water and carbon dioxide–water fluid inclusion standards. Following procedures outlined by Shepherd et al. (1985), the temperature of homogenization (T_h), temperature of first ice melting (T_{fm}), and final ice-melting temperature ($T_m ice$) were measured in two-phase liquid (L) + vapor (V) inclusions. During freezing at a cooling rate of 50°C/minute, the temperature at which the inclusions froze under metastable conditions (T_{mf}) was also recorded.

Due to the low measured homogenization temperature and high liquid content of the measured inclusions (>90% liquid at 25°C), fluid inclusion homogenization temperatures were recorded prior to low-temperature measurements in order to minimize the possible effects of stretching during freezing. The salts present in fluids were estimated by comparing recorded first ice melting temperatures with the known eutectic temperatures of common

aqueous-salt systems (Steele-MacInnis et al., 2016). In inclusions where the final ice-melting temperature was recorded, salinities were calculated for the water–sodium chloride system using the formula established by Bodnar (1993). Fluid salinities were also calculated based on the metastable freezing temperature using the equations of Wilkinson (2017). Although salinities calculated by metastable freezing temperatures likely have a higher degree of error (up to 3.2 eq. wt.% NaCl), they provide an estimate of fluid salinity in inclusions where vapor bubbles do not reappear prior to final ice melting. All fluid salinities are reported in weight % NaCl equivalent. Equivalent weight % NaCl is used as a measurement of salinity where precise speciation of salts in a sample has not been determined.

RESULTS

Description of Amethyst Mineralization. The amethyst found in the vein at La Manche occurs as scattered but locally abundant clusters in black clay found within a brecciated zone that appears to have formed in part from the subaerial weathering of calcite. The clusters are often loosened from the wall rock and may display broken points because of post-formation deformation. Three different types of amethyst can be found in the vein, sometimes close to each other but in different amethyst-lined cavities. The first is light purple to colorless and smaller than the other varieties, with an average crystal size of 1 cm (4 cm maximum). This has the least potential for gemstone cutting and mineral specimens due to its low color saturation and size. The remaining two amethyst varieties are more similar in size but vary in depth of color. One is saturated medium-dark purple in color (figure 5, A and B) while the other is saturated medium purple (figure 5C). Both varieties have significantly higher gemstone and specimen potential due to their more attractive appearance. These varieties are also much larger than the light purple amethyst to colorless quartz, with crystals averaging 2–3 cm in diameter and reaching up to 6 cm in maximum dimension. All coarsely crystalline quartz and amethyst observed at La Manche occurs only as a single final layer of mineralization in open cavities. Rarely, trace amounts of later colorless

Figure 5. Amethyst from La Manche. A: 9 cm wide with the largest crystal 4 cm tall. B: 11 cm wide. C: Medium purple amethyst, with the largest crystal measuring 4 cm wide. Photos by Philippe Belley.

Figure 6. A 32 × 7 mm polished section of amethyst from La Manche showing oscillatory zoning and weak sector zoning. The c-axis is indicated by the dashed line. Photo by Philippe Belley.

quartz (<2 cm) grow on top of the amethyst and generally show no preferential orientation with the underlying amethyst.

La Manche amethyst displays oscillatory and subtle sector zoning. A 7 mm thick cross section of medium-dark purple amethyst was cut and polished to display this zoning (figure 6). As is typical at La Manche, the outermost layer is colorless. The highest-quality gem material is generally found in the upper half to one-third of the crystals, from the broadest area to the termination. The edge of the amethyst crystals—where they contacted other crystals on the wall of a vug—tends to have an abundance of secondary fluid inclusions. Mineral inclusions (described in a subsequent section) are by far the most abundant in the final purple growth stage and the outer colorless zone.

Description of La Manche Amethyst Gemstones. Roughly half of the 357 faceted stones examined were light purple (all below 3 ct), and half were an attractive medium to medium-dark purple (with the most attractive color found in stones over 1 ct), while fewer than a dozen stones were colorless. The light purple stones were comparable in color to what is marketed as "rose de France" amethyst (figure 7, right faceted gem). While oscillatory and sector color zoning is present in La Manche amethyst, most faceted gemstones show uniform color when viewed table-up, though some examples show diffuse color

Figure 7. La Manche amethyst rough and faceted stones. The cut stone on the left (5.94 ct) shows diffuse color zoning. The one on the right (2.57 ct) is an example of light purple amethyst. Photo by Philippe Belley.

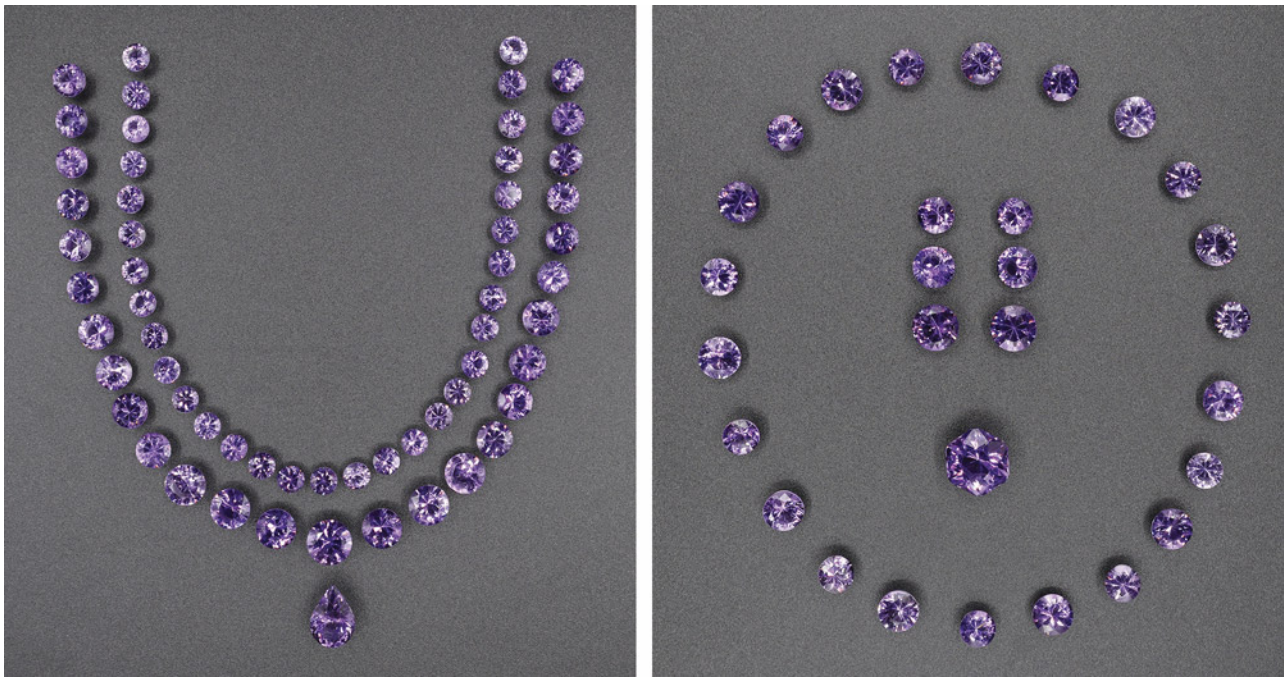

Figure 8. La Manche amethyst suite, 109.6 carats total. Left: Necklace set comprising round brilliants from 6 mm to 10 mm and a 3.69 ct pear cut. Right: Stones for a bracelet (7–8 mm rounds), earrings (7, 8, and 9 mm rounds), and a custom-cut hexagon (6.42 ct). Photos by Philippe Belley.

zoning where the depth of color changes slightly and progressively from one part of the stone to the other (figure 7, left faceted gem). The largest faceted gem examined weighed 6.42 ct, although an 11.0 ct oval faceted stone is known from the occurrence. Of particular note is a matching set of La Manche amethyst, 109.6 carats total (figure 8). The specific gravity, measured on a large transparent crystal fragment, was 2.66. Refractive indices, measured on three stones, were consistent: 1.541 (n_ω) and 1.550 (n_ε), with a birefringence of 0.009. Brazil twinning, a common feature in natural amethyst (Crowningshield et al., 1986), was generally visible in a simple polariscope, though sometimes difficult to observe depending on the orientation at which the gemstone was cut.

Fluid Inclusion Petrography and Microthermometry. Non-secondary fluid inclusions were rare, but FIA of primary, pseudosecondary, or indeterminate origin were observed in five of the seven samples studied. These were most common at the base and sides of the crystals, but some FIA of primary or indeterminate origin were also observed in the transparent and sparsely fractured amethyst near crystal terminations. Unequivocal primary FIA were observed in two samples, in trails parallel to the growth zones, and individual inclusions were generally elongate parallel to the *c*-axis growth direction (figure 9A). Pseudosecondary FIA were hosted in short trails that ran perpendicular to and terminated at growth zones. Indeterminate FIA occurred as clusters or short trails with no obvious relationship to growth zones.

Secondary FIA were observed in all samples and were much more abundant than other FIA types (>90% of total inclusions observed). They formed curvilinear trails (figure 9B) that crosscut growth zones and had a ribbon-like appearance parallel to the trend of the trail. Other secondary ribbon-like inclusions lined fractures that are not associated with secondary fluid inclusions (e.g., figure 9B): These can be difficult to observe when examining rough or preforms, and they can cause a stone to fracture during faceting (J. Henman, pers. comm., 2022).

Fluid inclusions hosted in primary, pseudosecondary, and indeterminate FIA were very similar in appearance and are described together. Inclusions ranged in size from <3 µm up to 30 µm. They were typically two-phase (liquid + vapor) at room temperature, but some monophase liquid inclusions were also observed. Two-phase inclusions were liquid rich with <10% vapor (figure 9, C and D) and did not show evidence of post-entrapment modification (i.e., leaking, stretching, decrepitation, necking down; Bodnar, 2003). All two-phase inclusions in individual FIA showed a consistent degree of fill. Secondary in-

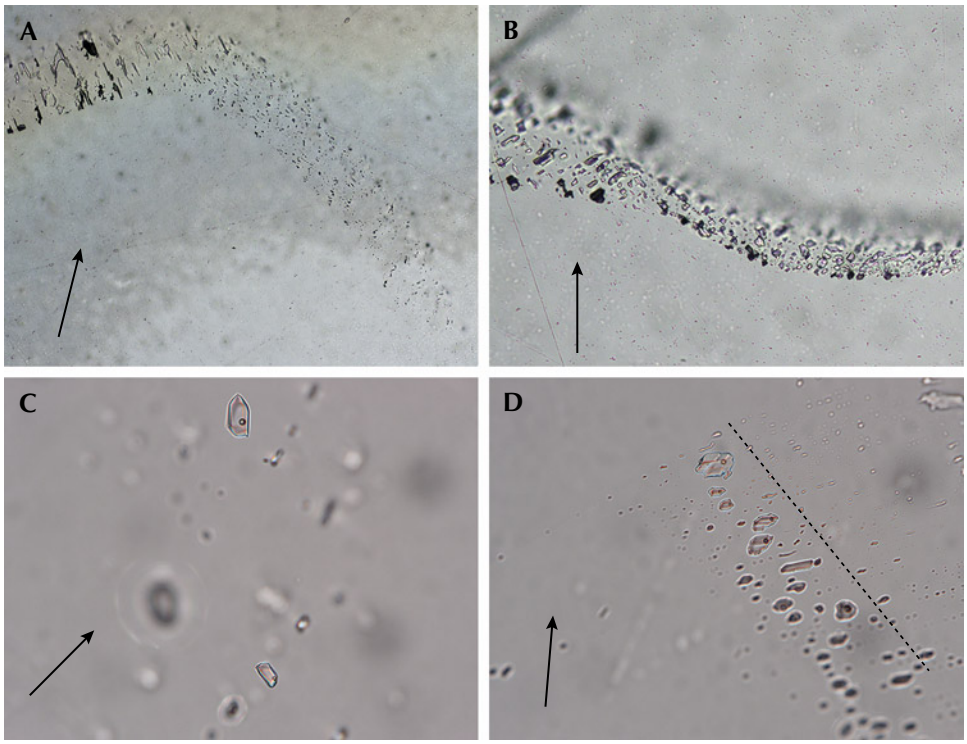

Figure 9. Fluid inclusions in La Manche amethysts viewed in transmitted light, with the arrow parallel to the c*-axis. A: Primary FIA in sample LM-Ame-01, located along a growth zone centered on what would be the point of the crystal. B: Secondary FIA in sample LM-Ame-01, occurring in a curvilinear, rehealed fracture. C: Typical two-phase (liquid + vapor) fluid inclusions in pseudosecondary FIA, sample LM-Ame-05. D: FIA of indeterminate origin in sample LM-Ame-07, with two-phase inclusions orientated perpendicular to the edge of the crystal (represented by dotted line). Photomicrographs by Joshua Maloney and James Conliffe; fields of view 1.11 mm (A), 0.36 mm (B), and 0.24 mm (C and D).*

clusions were smaller (<10 µm, generally <3 µm), and both monophase liquid and two-phase liquid-rich inclusions were observed. Some inclusions showed evidence of leaking with highly variable degrees of fill in individual FIA (monophase liquid to >20% vapor phase).

Microthermometric data recorded from 11 FIA in five samples is reported in table 1. Microthermometric data for inclusions hosted in primary, secondary, or indeterminate FIA was very similar (figure 10, left), and these results are reported together. Upon heating, all two-phase inclusions homogenized to the

Figure 10. Bivariate plots showing homogenization temperatures and salinities of amethyst from La Manche (this study) and associated sulfide, barite, and quartz-chlorite veins (Maloney, 1990). Data from individual FIA in amethyst showing average values with error bars denoting standard deviation.

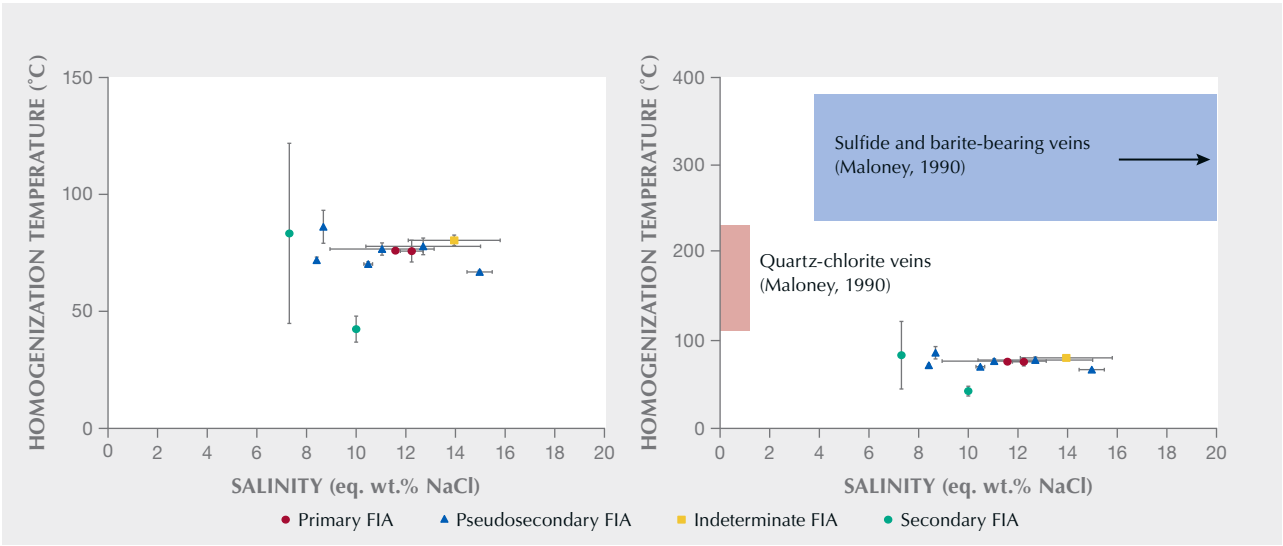

TABLE 1. Summary of fluid inclusion microthermometric data in amethyst from La Manche, Newfoundland.

Sample no.	Fluid inclusion assemblage	Setting	n[a]		T_{mf} (°C)	T_{fm} (°C)	$T_m$ice (°C)	Salinity (eq. wt.% NaCl)[b]	Salinity (eq. wt.% NaCl)[c]	T_h (°C)
LM-Ame-1	1	Primary	11	Avg	–52.0	–22.6	–8.5	12.2	10.0	75.7
				Std Dev[d]	0.0	na	0.4	0.5	0.0	4.6
	2	Secondary	6	Avg	–48.0	—	–4.6	7.3	6.9	83.3
				Std Dev	0.0	—	na	na	0.0	38.5
LM-Ame-4	1	Indeterminate	2	Avg	–58.2	–22.8	–5.9	9.1	13.9	80.4
				Std Dev	3.1	0.0	na	na	1.9	2.3
	2	Pseudosecondary	6	Avg	–53.1	–23.0	–7.0	10.5	10.8	70.2
				Std Dev	0.7	na	0.1	0.2	0.5	0.9
	3	Secondary	4	Avg	–52.0	—	—	—	10.0	42.4
				Std Dev	0.0	—	—	—	0.0	5.6
LM-Ame-5	1	Pseudosecondary	6	Avg	–59.8	–20.5	–4.1	6.6	15.0	66.9
				Std Dev	0.9	na	na	na	0.5	0.6
	2	Pseudosecondary	4	Avg	–56.3	–22.2	–8.1	11.8	12.7	77.8
				Std Dev	3.9	0.2	na	na	2.3	3.6
LM-Ame-6	1	Primary	2	Avg	–54.0	–21.1	–7.9	11.6	11.4	76.0
				Std Dev	0.0	0.1	na	na	0.0	1.1
	2	Pseudosecondary	7	Avg	–57.0	–21.0	–5.6	8.7	13.3	86.1
				Std Dev	0.0	na	na	na	0.0	7.0
LM-Ame-7	1	Indeterminate	5	Avg	–58.4	—	–5.4	8.4	14.1	71.9
				Std Dev	0.5	—	na	na	0.3	1.3
	2	Pseudosecondary	6	Avg	–53.7	—	—	—	11.0	76.6
				Std Dev	3.1	—	—	—	2.1	2.6

[a]*Number of inclusions analyzed in the assemblage*
[b]*Salinity calculated from* $T_m$ice *using equations of Bodnar (1993)*
[c]*Salinity calculated from* T_{mf} *using equations of Wilkinson (2017)*
[d]*Standard deviation of 0.0 indicates multiple inclusions with identical measured values; na indicates phase changes only observed in a single inclusion.*

liquid phase between 66.2° and 98.0°C (average 75.5°C, standard deviation 6.9°C, n = 47). Inclusions in individual FIA showed a narrow range of homogenization temperatures (generally <5°C), consistent with both trapping of a single-phase homogenous fluid and the absence of post-entrapment re-equilibration (Fall and Bodnar, 2018). Upon subsequent freezing at a rate of 50°C/minute, total freezing under metastable conditions occurred between –50° and –63°C. First ice melting (the eutectic temperature measured at the initiation of ice melting) was only observed in 10 inclusions between –23.0° and –20.5°C (average –21.9°C). These are close to the eutectic temperatures of pure H_2O-NaCl (–21.2°C) and H_2O-NaCl-KCl (–23°C) systems, indicating that NaCl (± KCl) is the most dominant salt in these inclusions, and they contain no significant amounts of $CaCl_2$ or $MgCl_2$ (Steele-MacInnis et al., 2016). Final ice melting, when no ice

Figure 11. A veil of secondary fluid inclusions along a rehealed fracture. Note the small black hematite spherulites. Photomicrograph by Philippe Belley; field of view 3.7 mm.

remains, in the presence of a vapor bubble was observed in 15 inclusions in the present study. This occurred between –8.7° and –4.1°C and was used to calculate fluid salinities between 6.6 and 12.5 eq. wt.% NaCl (average 10.7 eq. wt.% NaCl, standard deviation 1.8 eq. wt.% NaCl). In addition, fluid salinities from metastable ice melting temperatures were calculated using the equation of Wilkinson (2017). These range from 8.5 to 16.7 eq. wt.% NaCl (average 12.1 eq. wt.% NaCl, standard deviation 2.1 eq. wt.% NaCl), consistent with salinities calculated from $T_m ice$ and that the indicating fluids present during crystallization were of moderate salinity.

Microthermometric data was also collected from two secondary FIA to determine fluid flow history after crystal growth. They had a wide range of homogenization temperatures ranging from 38.0° to 144.0°C (homogenization to the liquid phase), with individual FIA having variations of >100°C indicating significant post-entrapment modification (i.e., leaking). Although eutectic temperatures were not observed, these inclusions freeze to form a clear ice before –50°C, suggesting that fluid compositions are dominated by NaCl ± KCl (Shepherd et al., 1985). A final ice melting temperature of –4.6°C was recorded in a single inclusion, corresponding to a salinity of 7.6 eq. wt.% NaCl and consistent with salinities calculated using metastable freezing temperatures (7.6 ± 1.1 eq. wt.% NaCl).

Inclusions in Faceted Stones. Due to their low abundance and generally very small size, primary fluid inclusions are rarely observed in cut gems using a standard gemological microscope. One rare example consisted of two very elongated primary fluid inclusions up to 1 mm long. Secondary fluid inclusions occur as subtle to prominent "veils" of inclusions along rehealed fractures. Subtle examples, consisting of relatively small and localized veils, occur commonly in faceted stones (figure 11). More prominent rehealed fractures are avoided by faceters but are common in amethyst crystals (e.g., figures 6 and 9).

La Manche amethyst contains multiple types of mineral inclusions that may occur together (figure 12) and are listed in order of abundance:

1. Black to red-orange spherical to globular hematite aggregates ("spherulites") from 5 to 100 µm in diameter (EDS confirmed against reference hematite and goethite samples mounted in the same polished puck; figure 12, A–C)
2. Needle-like and "beetle-leg" (figure 12B) to rod-like black to reddish inclusions that penetrate spherical aggregates, thought to be hematite
3. Radial bladed to acicular goethite clusters up to 1 mm long (EDS-confirmed)
4. Euhedral pyrite crystals showing complex habits, sometimes with parallel growth, up to 1 mm (EDS-confirmed; figure 12C)
5. Euhedral chalcopyrite crystals up to 0.4 mm (EDS-confirmed; figure 12D)

Hematite spherulites occur in many faceted stones. Like other mineral inclusions in La Manche amethyst, they are often restricted to one area of the faceted stone—the part of the outer zone of amethyst crystals that is richest in mineral inclusions. In most stones containing spherulites, these inclusions are only apparent upon close examination, especially with 10× magnification. Goethite and sulfide inclusions are less common and more prominently visible due to their larger average size.

DISCUSSION

Genetic Model. Layers of columnar calcite containing large, coarse-grained masses of galena in addition to dispersed barite clearly formed coevally: The minerals are found together in discrete layers of mineralization. Locally abundant masses of granular white quartz may also have formed in this stage, though no samples of this material were seen *in situ*. In many open cavities in the vein rock, barite occurs as later-stage layers where it is the dominant mineral preceding amethyst. Euhedral quartz crystals, generally as the amethyst variety, commonly overgrow the barite,

and barite has not been observed as intergrowths with quartz crystals. Therefore, amethyst crystallization occurred later than the other minerals in the vein. The restriction of amethyst to open cavities within layered calcite suggests that amethyst is a late-stage mineral genetically related to the lead-bearing hydrothermal veins. The presence of crystals with distinctive color, zoning, and sizes in separate but proximal pockets suggests the precipitation of quartz from trapped silica- and iron-bearing hydrothermal fluids where individual pockets behaved as relatively closed systems.

In a fluid inclusion study of barite-, sulfide-, and quartz-bearing veins in the Avalon Peninsula, Maloney (1990) found that sulfide-bearing and barite-bearing veins formed between 240°–370°C, with moderate to high salinity (~4.5–39 eq. wt.% NaCl, which includes NaCl, $CaCl_2$, and $MgCl_2$). In contrast, quartz-chlorite veins in the region formed as a result of regional low-grade metamorphism, where fluid inclusions have homogenization temperatures in the 110°–230°C range and extremely low salinity (average 0.6 eq. wt.% NaCl; Maloney, 1990). Fluid inclusion data from amethyst shows much lower homogenization temperatures (75.5° ± 6.9°C) relative to sulfide-barite-calcite in the region, as well as quartz-chlorite veins not associated with sulfide mineralization (figure 10, right). Although these homogenization temperatures represent minimum trapping temperatures, the low-grade regional metamorphism and open vuggy nature of the amethyst veins suggest that formation took place at relatively shallow crustal levels and the formation temperature of the La Manche amethyst was relatively low compared to other barite-, sulfide-, and quartz-bearing veins in the Avalon Peninsula. The salinity of fluid in primary inclusions in amethyst is considerably higher than in fluid in the quartz-chlorite veins, and

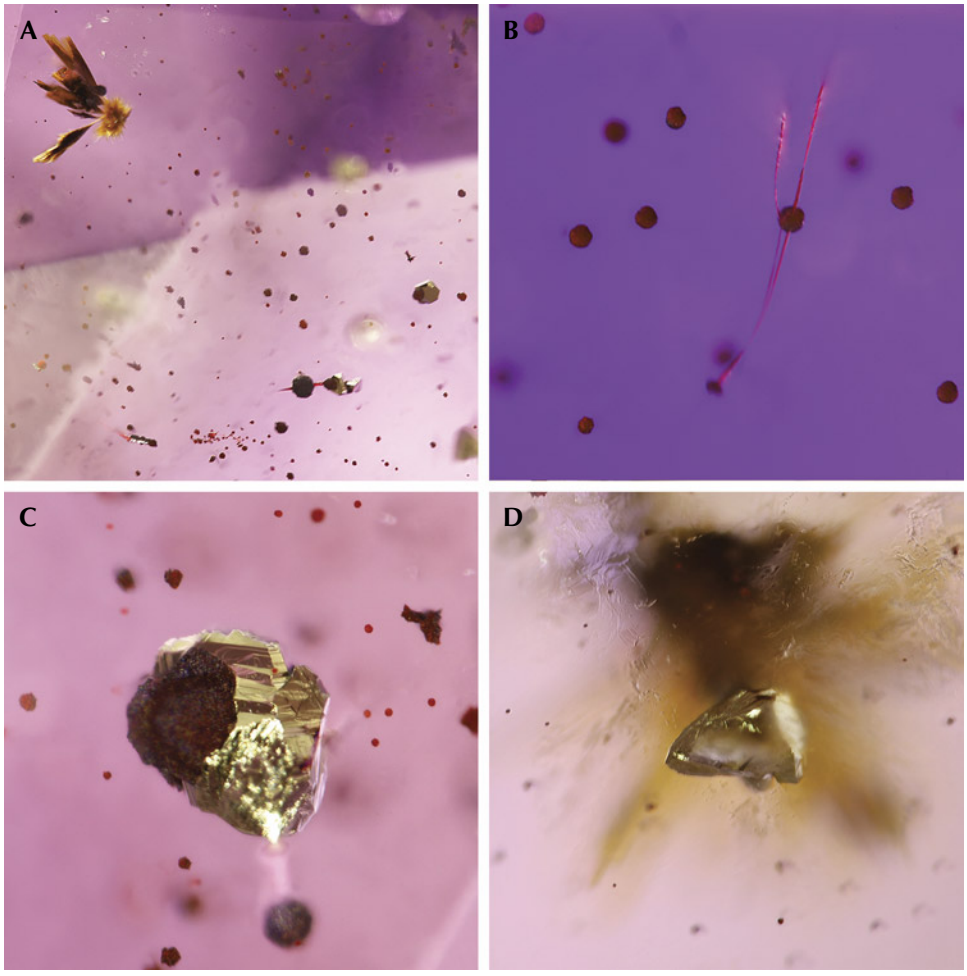

Figure 12. Mineral inclusions in La Manche amethyst. A: A cluster of acicular ochre goethite, black to red hematite spherulites, and euhedral sulfide crystals. B: Thin wiry "beetle-leg" type inclusion (probably hematite) associated with hematite spherulites in the emerald-cut gemstone pictured in figure 7. C: Pyrite showing parallel growth features in association with hematite. D: Pseudo-tetrahedral chalcopyrite crystal associated with goethite and hematite in amethyst. The color of the chalcopyrite inclusion was not apparent until it was later exposed by polishing and verified with reflected light microscopy and EDS. Photomicrographs by Philippe Belley; fields of view 2.10 mm (A), 0.77 mm (B), 0.80 mm (C), and 0.70 mm (D).

within the range of the ones associated with sulfide and barite veins. Therefore, vein structure, mineral textural relationships, and primary fluid inclusion homogenization temperatures and salinity suggest that La Manche amethyst formed in the final stage of mineral deposition by hydrothermal fluids at relatively low temperature (likely <100°C).

The thin colorless quartz rims on La Manche amethyst are an interesting feature. In the light purple amethysts, the purple zone is relatively small and limited to the core of the crystal, while the colorless layer is relatively thick (up to 80% of the crystal's radius). In the crystal-lined pockets of greatest commercial interest, most of the amethyst is medium to medium-dark purple in color with only a thin colorless rim (<20% of the crystal's radius). In all examples, iron-rich mineral inclusions (hematite, goethite, sulfides) occur principally in the outer purple zone as it transitions into colorless. Since amethyst color is generated by an interstitial Fe^{3+} impurity in quartz, we hypothesize that changing physicochemical conditions led to the precipitation of dissolved iron, and therefore iron was no longer available in the mineralizing fluids during the final stages of amethyst/quartz growth.

Comparison of Mineral Inclusions to Other Sources. Some primary inclusions in La Manche amethyst are common in amethyst from numerous sources, in particular "beetle-leg" habit black or reddish strands (likely hematite) and radiating aggregates of ochre-colored bladed to acicular goethite (see summary in table 2 and references therein). These inclusions are known to occur in amethyst in epigenetic hydrothermal veins (both hematite and goethite), geodes in basalt (goethite only), pockets in pegmatites (hematite only), and miarolitic cavities (hematite only; see table 2). Some inclusions known from basalt-hosted amethyst geode deposits (fluorite, calcite, and anhydrite; Gilg et al., 2003; Hyršl, 2006) and volcanic/volcaniclastic-hosted epithermal occurrences (microcline and baryte; Voudouris et al., 2018) were not observed at La Manche. The amethyst deposit containing the most similar inclusion assemblage is in Thunder Bay, Ontario, Canada, which (like La Manche) contains spherulitic hematite, acicular goethite, as well as pyrite and chalcopyrite (Kile, 2019). Hematite spherulites at Thunder Bay are generally reddish and occur in very high concentrations in late growth layers of some amethyst, causing an opaque red-brown coloration (Kile, 2019)—a significant contrast to the dominantly black color (likely due to larger crystallite size) and localized but low density of hematite spherulite inclusions in La Manche amethyst. The crystal habit of sulfides also differs between these two Canadian localities. Pyrite inclusions are cubic at Thunder Bay, while at La Manche they are either flattened or have more complex morphology (showing a combination of cubic, octahedral, and possibly pyritohedral faces). At Thunder Bay, chalcopyrite occurs as aggregates of fine-grained crystals (Kile, 2019), while at La Manche they occur as individual euhedral crystals. Sulfides are, however, very uncommon as inclusions in La Manche amethyst and therefore unlikely to be a useful discriminator of origin. The species and habit of more common mineral inclusions in La Manche amethyst overlap significantly with numerous other deposits.

Factors Affecting Amethyst Quality. A number of factors impact the quality of the amethyst found in the La Manche vein and affect their value as gemstones and specimens. In terms of primary features, the color zoning in amethyst results in faceted gemstones of varying lightness and saturation, with the more sought-after medium-dark intense purple as well as the lighter-colored "rose de France" type of amethyst. Some faceted stones contain small clusters of tiny hematite spherulites that are visible without magnification or under low magnification, but these are usually not apparent without close inspection.

The most significant factors affecting gem quality are secondary: Post-crystallization deformation has resulted in the formation of common rehealed fractures that contain secondary fluid inclusions, and post-formation pocket collapse resulted in damaged points on some mineral specimens. With regard to secondary fluid inclusions, the temperature of formation and salinity are unclear, but it is possible that they were formed by a relatively low-salinity fluid not related to hydrothermal mineralization.

Considering these factors, the La Manche occurrence has produced numerous beautiful faceted stones and mineral specimens with only minor test sampling. Its amethysts far surpass those from Thunder Bay with regard to the abundance of transparent facet-quality material (Wilson, 2014).

Geological Comparison with Other Deposits. Amethyst deposits are divided into the following categories:

1. Epigenetic hydrothermal veins, where mineralization crosscuts diverse rock types (e.g.,

TABLE 2. Summary of mineral inclusion types and fluid inclusion data in amethyst from La Manche, Newfoundland, and other localities.[a]

		Deposit type						
		Epigenetic hydrothermal veins						
Mineral inclusions	**Habit**	**Canada (La Manche)**	**Canada (Thunder Bay)**	**Brazil[b]**	**Kazakhstan[b]**	**Madagascar[b]**	**Morocco (Boudi)**	**Rwanda[b]**
Hematite	Acicular	x		x	x	x	x	x
	Spherulites	x	x					
	Flakes							
	Dendrites							
Goethite	Acicular/sprays	x	x	x	x	x		
Pyrite	Cubes		x					
	Complex forms	x						
	Platy	x						
Chalcopyrite	Single crystals	x						
	Crystal aggregates		x					
Fluorite								
Calcite								
Anhydrite								
Baryte								
Cristobalite								
Microcline								
Hydrocarbon	(liquid secondary inclusions)							
Fluid Inclusions								
Primary and Pseudosecondary	T_h (°C)	66.9–86.1	40.0–91.2	—	—	—	154–330	—
	Salinity (NaCl eq. wt.%)	10.0–15.0	15.3–22.9	—	—	—	5.7–13.9	—
Secondary	T_h (°C)	42.4–83.3	—	—	—	—	—	—
	Salinity (NaCl eq. wt.%)	6.9–10.0	—	—	—	—	—	—

[a]*Data sources: Yang et al. (2001); Gilg et al. (2003, 2014); Lowell and Koivula (2004); Hyršl (2006); Morteani et al. (2010); Commin-Fischer et al. (2010); Troilo et al. (2015); Dumańska-Słowik (2017); Feely et al. (2017); Schmetzer and Williams (2018); Voudouris et al. (2018); Kile (2019); Dias et al. (2021).*
[b]*Only the deposit type and country of origin are listed for these occurrences by Hyršl (2006).*
[c]*Hydrothermal breccia in granite*

TABLE 2 (continued). Summary of mineral inclusion types and fluid inclusion data in amethyst from La Manche, Newfoundland, and other localities.[a]

		Deposit type					
		Epigenetic hydrothermal veins			Geodes in basalt	Pegmatite	Miarolitic cavities
Mineral inclusions	**Habit**	**United States (Four Peaks, Arizona)**	**United States[c] (Green Ridge, Washington)**	**Greece (various occurrences)**	**Brazil/ Uruguay**	**Brazil[b]**	**South Korea**
Hematite	Acicular					x	x
	Spherulites						
	Flakes	x					
	Dendrites						x
Goethite	Acicular/sprays			x	x		
Pyrite	Cubes						
	Complex forms						
	Platy						
Chalcopyrite	Single crystals						
	Crystal aggregates						
Fluorite					x		
Calcite					x		
Anhydrite					x		
Baryte				x			
Cristobalite					x		
Microcline				x			
Hydrocarbon	(liquid secondary inclusions)		x				
Fluid Inclusions							
Primary and Pseudosecondary	T_h (°C)	—	270–311	189–275	50–120	—	273–288
	Salinity (NaCl eq. wt.%)	—	5.4–9.5	0.9–8.0	0.3–5.3	—	4
Secondary	T_h (°C)	—	—	—	—	—	—
	Salinity (NaCl eq. wt.%)	—	—	—	—	—	—

[a]*Data sources: Yang et al. (2001); Gilg et al. (2003, 2014); Lowell and Koivula (2004); Hyršl (2006); Morteani et al. (2010); Commin-Fischer et al. (2010); Troilo et al. (2015); Dumańska-Słowik (2017); Feely et al. (2017); Schmetzer and Williams (2018); Voudouris et al. (2018); Kile (2019); Dias et al. (2021).*
[b]*Only the deposit type and country of origin are listed for these occurrences by Hyršl (2006).*
[c]*Hydrothermal breccia in granite*

Kievlenko, 2003; Lowell and Koivula, 2004; Troilo et al., 2015; Dumańska-Słowik et al., 2017; Voudouris et al., 2018; Kile, 2019), sometimes also as hydrothermal breccias (Feely et al., 2017)
2. Basalt-hosted deposits, where amethyst is precipitated from hydrothermal fluid in geodes (Gilg et al., 2003, 2014; Morteani et al., 2010; Commin-Fischer et al., 2010; Dias et al., 2021)
3. Pegmatites and miarolitic cavities, in which late-stage amethyst crystallizes from hydrothermal fluids in the final stages of magmatic crystallization (e.g., Yang et al., 2001; Kievlenko, 2003)
4. Skarns, where amethyst forms in vugs as a late-stage mineral (Ontiveros et al., 2004)

Epigenetic hydrothermal amethyst deposits, such as that at La Manche, form in faults, joints, or breccias, often in rocks experiencing structural extension that creates structures along which hydrothermal fluids can travel. Most epigenetic hydrothermal vein-type amethyst deposits are nearly monomineralic (with the exception of some Russian deposits containing locally abundant calcium and iron carbonates; Kievlenko, 2003), and multiple growth stages of quartz deposition—often colorless, smoky, and later-stage amethyst—occur successively (Epstein, 1988; Garland, 1994; Kievlenko, 2003; Lowell and Koivula, 2004). The association of amethyst with an epigenetic hydrothermal base metal sulfide deposit at La Manche (galena with minor sphalerite and chalcopyrite; Maloney, 1990) is more similar to mineralization at Thunder Bay and at the Madjarovo gold-polymetallic deposit in Bulgaria. The La Manche occurrence is distinct in that individual quartz- or amethyst-lined pockets only contain one generation of crystals, with no repeated layers of quartz as found in many other hydrothermal deposits such as Thunder Bay and Madjarovo.

Two types of amethyst-bearing veins occur in the Thunder Bay area (Garland, 1994). In the west, amethyst is a minor constituent in vein systems consisting of three stages of mineralization: (A) calcite + sulfides; (B) quartz, including amethyst (if present); and (C) barite and fluorite (if present), with small quantities of silver-bearing minerals. In the east, there are notable amethyst deposits consisting of layers of white sugary quartz transitioning to episodic bands of white, smoky, and amethyst quartz, with sulfide minerals (galena, chalcopyrite, pyrite, and sphalerite) forming sparse lenses below the final layers of amethyst and occasionally containing late barite or fluorite overgrowths on euhedral amethyst (Garland, 1994; Kile, 2019). Gem-quality amethyst at Thunder Bay is extremely rare, and facet-quality material has only been reported from the quartz/amethyst-dominated type of vein (see Wilson, 2014). It is important to highlight that barite at Thunder Bay generally formed later than the amethyst, while it formed exclusively prior to amethyst deposition at La Manche. Furthermore, amethyst pockets at La Manche are enclosed within host calcite in the main vein, while the largest and most commercially important pockets in Thunder Bay occur at intersections between sets of mineralized faults (Garland, 1994).

In the Madjarovo deposit of Bulgaria, the crystallization of prismatic amethyst crystals occurred at the end of the hydrothermal process, with amethyst postdating copper, lead, and zinc sulfide mineralization in the same vein (Kievlenko, 2003, and references therein). The formation of amethyst in the final stage of mineral precipitation from hydrothermal fluids in a base metal sulfide deposit is common to both Madjarovo and La Manche. However, late-stage quartz in the Madjarovo deposit occurs as multiple discrete layers, a common feature in most amethyst deposits that is absent at La Manche. Principal gangue minerals at Madjarovo are quartz and calcite, whereas the dominant gangue mineral at La Manche is calcite with subordinate barite and locally abundant quartz that was not observed *in situ*.

The occurrence of amethyst in the latest stage of quartz growth is likely due to its relatively low temperature of formation (approximately 40°–250°C) and to the occurrence of oxidizing conditions required to form trivalent iron, which causes the purple color when incorporated into quartz and subsequently exposed to natural background radiation (Dennen and Pucket, 1972; Cohen, 1985; McArthur et al., 1993; Morteani et al., 2010). Amethyst crystallization at La Manche occurred at relatively low temperatures (<100°C), comparable to formation temperatures at Thunder Bay (range 40.0°–91.2°C, average 68.4°C), and lower than at Madjarovo and the numerous Russian deposits (100°–220°C; Kievlenko, 2003). The fluid inclusion entrapment temperature at La Manche is also lower than for amethyst in epithermal occurrences in Greece (approximately 200°–250°C; Voudouris et al., 2018) and New Zealand (170°–253°C; Braithwaite and Faure, 2002). The high-

est temperatures determined for two-phase fluid inclusions in a hydrothermal vein–type deposit are in the Boudi deposit in Morocco (154°–330°C; Dumańska-Słowik et al., 2017), and temperatures of 273°–288°C are known in amethyst from miarolitic cavities (Yang et al., 2001). Gilg et al. (2003) suggests a similar low formation temperature (<100°C) for geode-hosted amethyst in basalt (Brazil), but this is contradicted by estimates of 152°–238°C in primary fluid inclusions by Proust and Fontaine (2007). However, most fluid inclusions in Brazilian/Uruguayan basalt-hosted amethyst are monophase, and the two-phase inclusions used by Proust and Fontaine (2007) may have leaked, giving unreliable results, which is supported by the low formation temperatures inferred from oxygen isotope data (Gilg et al., 2014). In the basalt-hosted amethyst in Uruguay, Morteani et al. (2010) estimated formation temperatures between 50° and 120°C.

Hydrothermal fluid salinity at La Manche is moderate (10.7 ± 1.8 eq. wt.% NaCl), which is comparable to higher values from Boudi (5.7–13.9 eq. wt.% NaCl; Dumańska-Słowik et al., 2017) and epithermal amethyst occurrences in Greece (0.9–8.0 eq. wt.% NaCl; Voudouris et al., 2018), and significantly higher than in geode-type basalt-hosted amethyst in Brazil (0.3–5.3 eq. wt.% NaCl; Gilg et al., 2014) and epithermal amethyst in New Zealand (≤4.5 eq. wt.% NaCl; Braithwaite and Faure, 2002). Amethyst from miarolitic cavities in aplite cutting granite at the Eonyang deposit in South Korea contains lower-salinity fluid inclusions (4 eq. wt.% NaCl) that also contain CO_2 as well as H_2O and NaCl (Yang et al., 2001). Amethyst in Thunder Bay formed in fluids containing a higher salinity than all the aforementioned deposits, ranging between 15.3 and 22.9 eq. wt.% NaCl (McArthur et al., 1993).

Figure 13. The second- and third-largest faceted stones produced from the La Manche amethyst occurrence to date: 9.09 ct (left) and 8.46 ct (right). Photo by Philippe Belley.

CONCLUSIONS

La Manche amethyst features a range of colors, including saturated medium to medium-dark purple and light purple. The deposit has produced numerous beautiful faceted gemstones in exploration test samples, with a few as large as 8–11 carats (figure 13). The occurrence is a new example of an epigenetic hydrothermal-type deposit and one of the few examples where amethyst formed as a final-stage hydrothermal mineral in open cavities within a vein-hosted base metal sulfide deposit. La Manche is different from most vein-hosted amethyst deposits in that vugs generally contain only one discrete layer of amethyst rather than multiple banded layers—and the fact that this layer primarily occurs over calcite and barite. Based on microthermometry of two-phase primary inclusions, amethyst at La Manche formed at relatively low temperature (<100°C) and moderate salinity dominated by NaCl (approximately 11 eq. wt.% NaCl). It contains mineral inclusions similar to those found in many other deposits (i.e., acicular and spherulitic hematite and radiating acicular goethite) as well as others known only from the Thunder Bay deposits (pyrite and chalcopyrite). Pyrite and chalcopyrite inclusions in La Manche amethyst are relatively rare and can be differentiated by morphology from those reported in Thunder Bay amethyst. Due to the similar appearance of La Manche faceted amethyst gemstones to that from other sources, and the scarcity of inclusions unique to La Manche, they cannot be reliably differentiated. Origin would therefore require to be certified by mine-to-market supply chain management.

ABOUT THE AUTHORS

Joshua Maloney is a recent graduate of the B.Sc. Honours Geology program at Memorial University of Newfoundland (MUN), St. John's, Canada, and is now working as an exploration geologist. Dr. Philippe Belley is an assistant professor and manages the Gem Science Research Group at MUN. Dr. James Conliffe is a project geologist in the Mineral Deposits Section, Department of Mines & Energy, Government of Newfoundland and Labrador.

ACKNOWLEDGMENTS

The authors are extremely grateful for the support of claim owner Jason White, who guided multiple site visits, allowed sampling, and shared information. We thank Jaimy Henman for precision faceting the gemstones in figure 7 and providing feedback on the material, Andrea Mills (Government of Newfoundland and Labrador) for providing a high-resolution copy of the geological map of the Avalon Peninsula, Matt Crocker (MUN) for polished section preparation, and Dylan Goudie (MUN) for help with SEM-EDS.

REFERENCES

Bodnar R.J. (1993) Revised equation and table for determining the freezing point depression of H_2O-NaCl solutions. *Geochimica et Cosmochimica Acta*, Vol. 57, No. 3, pp. 683–684, http://dx.doi.org/10.1016/0016-7037(93)90378-A

——— (2003) Reequilibration of fluid inclusions. In I. Samson, et al., Eds., *Fluid Inclusions: Analysis and Interpretation*. Mineralogical Association of Canada, Short Course Series 32, pp. 1–8.

Braithwaite R.L., Faure K. (2002) The Waihi epithermal gold-silver-base metal sulfide-quartz vein system, New Zealand: Temperature and salinity controls on electrum and sulfide deposition. *Economic Geology*, Vol. 97, No. 2, pp. 269–290, http://dx.doi.org/10.2113/gsecongeo.97.2.269

Cohen A.J. (1985) Amethyst color in quartz, the result of radiation protection involving iron. *American Mineralogist*, Vol. 70, No. 11-12, pp. 1180–1185.

Colman-Sadd S.P., Hayes J.P., Knight I. (1990) Geology of the Island of Newfoundland (digital version of Map 90-01); Scale: 1:1,000,000. Government of Newfoundland and Labrador, Department of Mines and Energy, Geological Survey Branch. Open File GS# NFLD/2192.

Commin-Fischer A., Berger G., Polvé M., Dubois M., Sardini P., Beaufort D., Formoso M. (2010) Petrography and chemistry of SiO_2 filling phases in the amethyst geodes from the Serra Geral Formation deposit, Rio Grande do Sul, Brazil. *Journal of South American Earth Sciences*, Vol. 29, No. 3, pp. 751–760, http://dx.doi.org/10.1016/j.jsames.2009.10.002

Crowningshield R., Hurlbut C., Fryer C.W. (1986) A simple procedure to separate natural from synthetic amethyst on the basis of twinning. *G&G*, Vol. 22, No. 3, pp. 130–139, http://dx.doi.org/10.5741/GEMS.22.3.130

Dennen W.H., Puckett A.M. (1972) On the chemistry and color of amethyst. *Canadian Mineralogist*, Vol. 11, pp. 448–456.

Dias C.H., de Sa Carneiro Chaves M.L., Figueiredo e Silva R.C., Dutra Gomes S. (2021) Fluid inclusions in amethyst quartz of different geological environments from Brazil. *Mineralogical Magazine*, Vol. 85, No. 3, pp. 332–347, http://dx.doi.org/10.1180/mgm.2021.38

Dumańska-Słowik M., Toboła T., Jarmołowicz-Szulc K., Naglik B., Dylag J., Szczerba J. (2017) Inclusion study of hourglass amethyst from Boudi (Morocco) by Raman microspectroscopy and microthermometric measurements. *Spectrochimica Acta Part A: Molecular and Biomolecular Spectroscopy*, Vol. 187, pp. 156–162, http://dx.doi.org/10.1016/j.saa.2017.06.053

Epstein D.S. (1988) Amethyst mining in Brazil. *G&G*, Vol. 24, No. 4, pp. 214–228, http://dx.doi.org/10.5741/GEMS.24.4.214

Feely M., Costanzo A., Lindner F., George J., Parnell J., Bowden S., Baba M., Owens P. (2017) Quartz-amethyst hosted hydrocarbon-bearing fluid inclusions from the Green Ridge Breccia in the Snoqualmie Granite, North Cascades, WA, USA. *Minerals*, Vol. 7, No. 9, article no. 174, http://dx.doi.org/10.3390/min7090174

Garland M.I. (1994) Amethyst in the Thunder Bay area. Ontario Geological Survey, Open File Report 5891, 197 pp.

Gilg H.A., Krüger Y., Taubald H., van den Kerkhof A.M., Frenz M., Morteani G. (2014) Mineralisation of amethyst-bearing geodes in Ametista do Sul (Brazil) from low-temperature sedimentary brines: Evidence from monophase liquid inclusions and stable isotopes. *Mineralium Deposita*, Vol. 49, No. 7, pp. 861–877, http://dx.doi.org/10.1007/s00126-014-0522-7

Gilg H.A., Morteani G., Kostitsyn Y., Preinfalk C., Gatter I., Strieder A.J. (2003) Genesis of amethyst geodes in basaltic rocks of the Serra Geral Formation (Ametista do Sul, Rio Grande do Sul, Brazil): A fluid inclusion, REE, oxygen, carbon, and Sr isotope study on basalt, quartz, and calcite. *Mineralium Deposita*, Vol. 38, No. 8, pp. 1009–1025, http://dx.doi.org/10.1007/s00126-002-0310-7

Goldstein R.H. (2003) Petrographic analysis of fluid inclusions. In I. Samson et al., Eds., *Fluid Inclusions: Analysis and Interpretation*, Mineralogical Association of Canada, Short Course Series 32, pp. 9–54.

Howley J.P. (2009) *Reminiscences of Forty-Two Years of Exploration in and About Newfoundland*. Edited by W.J. Kirwin and P.A. O'Flaherty. Memorial University of Newfoundland, St. John's, Canada. 2053 pp.

Hyršl J. (2006) Gemological Abstracts: Genetic classification of mineral inclusions in quartz. *G&G*, Vol. 42, No. 3, pp. 97–98.

Kievlenko E.Y. (2003) *Geology of Gems*, English edition. Ocean Pictures Ltd., Littleton, Colorado.

Kile D.E. (2019) Mineralogy of the amethyst mines in the Thunder Bay area, Thunder Bay, Ontario, Canada. *Rocks & Minerals*, Vol. 94, No. 4, pp. 306–343, http://dx.doi.org/10.1080/00357529.2019.1595939

Lowell J., Koivula J.I. (2004) Amethyst from Four Peaks, Arizona. *G&G*, Vol. 40, No. 3, pp. 230–238, http://dx.doi.org/10.5741/GEMS.40.3.230

Maloney J.A. (1990) The origin of barite and related veins on the Avalon Peninsula of Newfoundland. Unpublished master's thesis, Memorial University of Newfoundland. St. John's, Canada.

McArthur J.R., Jennings E.A., Kissin S.A., Sherlock R.L. (1993) Stable-isotope, fluid-inclusion, and mineralogical studies relating to the genesis of amethyst, Thunder Bay Amethyst Mine, Ontario. *Canadian Journal of Earth Sciences*, Vol. 30, No. 9, pp. 1955–1969, http://dx.doi.org/10.1139/e93-172

Mills A.J., Dunning G.R., Langille A. (2016) New geochronological

constraints on the Connecting Point Group, Bonavista Peninsula, Avalon Zone, Newfoundland. In *Current Research*, Newfoundland and Labrador Department of Natural Resources, Geological Survey, Report 16-1, pp. 153–171.
Mills A.J., Dunning G.R., Sandeman H.A. (2021) Lithogeochemical, isotopic, and U-Pb (zircon) age constraints on arc to rift magmatism, northwestern and central Avalon Terrane, Newfoundland, Canada; implications for local lithostratigraphy. *Canadian Journal of Earth Sciences*, Vol. 58, No. 4, pp. 332–354, http://dx.doi.org/10.1139/cjes-2019-0196
Morteani G., Kostitsyn Y., Preinfalk C., Gilg H.A. (2010) The genesis of the amethyst geodes at Artigas (Uruguay) and the paleohydrology of the Guaraní aquifer: Structural, geochemical, oxygen, carbon, strontium isotope and fluid inclusion study. *International Journal of Earth Sciences*, Vol. 99, pp. 927–947, http://dx.doi.org/10.1007/s00531-009-0439-z
Murray A. (1869) *Report upon the Geological Survey of Newfoundland for the Year 1868*. Robert Winton, printer to the Hon. House of Assembly, St. John's, Newfoundland, Canada, 68 pp.
O'Brien S.J., Dunning G.R., Knight I., Dec T. (1989) Late Precambrian geology of the north shore of Bonavista Bay (Clode Sound to Lockers Bay). Government of Newfoundland and Labrador, Department of Mines, Geological Survey Report of Activities, pp. 49–50.
Ontiveros M., Wilson W.E., Megaw P.K.M. (2004) Famous mineral localities: The Guerrero amethyst deposits, Mexico. *Mineralogical Record*, Vol. 35, No. 6, pp. 29–37.
Papezik V.S. (1974) Prehnite-pumpellyite facies metamorphism of late Precambrian rocks of the Avalon Peninsula, Newfoundland. *Canadian Mineralogist*, Vol. 12, pp. 463–468.
Proust D., Fontaine C. (2007) Amethyst geodes in the basaltic flow from Triz quarry at Ametista do Sul (Rio Grande do Sul, Brazil): Magmatic source of silica for the amethyst crystallizations. *Geological Magazine*, Vol. 144, No. 4, pp. 731–739, http://dx.doi.org/10.1017/S0016756807003457
Schmetzer K., Williams B. (2018) Gem-quality amethyst from Rwanda: Optical and microscopic properties. *Journal of Gemmology*, Vol. 36, No. 1, pp. 26–36.
Shepherd T.J., Rankin A.H., Alderton D.H.M. (1985) *A Practical Guide to Fluid Inclusions*. Blackie, London.
Steele-MacInnis M., Ridley J., Lecumberri-Sanchez P., Schlegel T.U., Heinrich C.A. (2016) Application of low-temperature microthermometric data for interpreting multicomponent fluid inclusion compositions. *Earth-Science Reviews*, Vol. 159, pp. 14–35, http://dx.doi.org/10.1016/j.earscirev.2016.04.011
Tibbo H.G. (1983) Report on a diamond drilling program on mineral claim 12072, License No. 12014, La Manche Project, Placentia Bay, Newfoundland. Tasu Resources Ltd., Newfoundland and Labrador exploration report file 001N-0448.
Troilo F., El Harfi A., Mouaddib S., Bittarello E., Costa E. (2015) Amethyst from Boudi, Morocco. *G&G*, Vol. 51, No. 1, pp. 32–40, http://dx.doi.org/10.5741/GEMS.51.1.32
Voudouris P., Melfos V., Mavrogonatos C., Tarantola A., Götze J., Alfieris D., Maneta V., Psimis I. (2018) Amethyst occurrences in Tertiary volcanic rocks of Greece: Mineralogical, fluid inclusion and oxygen isotope constraints on their genesis. *Minerals*, Vol. 8, No. 8, article no. 324, http://dx.doi.org/10.3390/min8080324
Wilkinson J.J. (2017) Metastable freezing: A new method for the estimation of salinity in aqueous fluid inclusions. *Economic Geology*, Vol. 112, No. 1, pp. 185–193, http://dx.doi.org/10.2113/econgeo.112.1.185
Wilson B.S. (2020) Colored gemstones from Canada: An update. *InColor*, No. 45, pp. 78–85.
——— (2014) Colored gemstones from Canada. In L.A. Groat, Ed., *Geology of Gem Deposits*, 2nd ed., Mineralogical Association of Canada, Short Course Series 44, pp. 375–405.
Yang K.H., Yun S.H., Lee J.D. (2001) A fluid inclusion study of an amethyst deposit in the Cretaceous Kyongsang Basin, South Korea. *Mineralogical Magazine*, Vol. 65, No. 4, pp. 477–487, http://dx.doi.org/10.1180/002646101750377515